J. Lorenzo, A. Lázaro, R. Villarino and D. Girbau. “Modulated Frequency Selective Surfaces for Wearables RFID and Sensors Applications”, IEEE Transaction on Microwave Theory and Techniques, vol. 64(10), pp. 4447-4456, October 2016.

doi: 10.1109/tap.2016.2596798

URL: https://ieeexplore.ieee.org/document/7527641

Modulated Frequency Selective Surfaces for wearable RFID and sensor applications

J.Lorenzo, A.Lazaro, *Member, IEEE* , R.Villarino, D.Girbau, *Senior Member, IEEE*

***Abstract*—This paper presents a transponder based on a modulated frequency selective surface as an alternative based on backscattering communication for wearable applications. The transponder is composed of an array of dipoles loaded with varactor diodes to modulate the backscatter response. The information is obtained by changing the cross section of the frequency selective surface. The detuning and the power loss of the transponder when in contact with the body are studied. Several frequency selective surfaces with different number of dipoles and placed on different surfaces are studied, as a proof of concept. In addition, a temperature sensor for on-body applications is proposed. The reader is also presented and experimental results are provided.**

***Index Terms*— Frequency selective surface, wireless body area networks, wireless sensor networks, radiofrequency identification, backscattering.**

I. Introduction

A WIRELESS body area network (WBAN) is a wireless network used for communication among sensor nodes operating on, in contact, or close to the human body. WBAN have recently been subject to great interest not only in medical applications but also as an enabling technology for users in lifestyle, assisted living, sports and entertainment [1]. This technology has several challenges. One of these is the overall size and weight of the devices that have to be tailored on the body in order to avoid disturbances in human activity. This requires new integration technologies that are commonly known as wearable technologies. Another important challenge is the total energy consumption of the sensor nodes, with a direct impact on autonomy. The extreme case can be observed in implantable devices. Significant efforts have been made in this area, integrating different energy harvesting methods to extend battery life or producing autonomy sensors [2]. Small and very low-profile antennas for on-body applications are in great demand in the field of WBAN [3][4] and in radiofrequency identification (RFID) tags for wearable applications [5][6]. Some examples of textile antennas are given in [7][8][9][10]. The proximity of the body may easily reduce the efficiency and detune the antennas [10]. Special antenna design techniques are therefore required, and special attention must also be paid when calculating the link budget [11]. In fact, several works analyze the radio channel for BAN applications [11][12][13]. In order to increase the reliability of the communication link, approaches based on diversity concept have been proposed to reduce the impact of attenuation [14].

Frequency Selective Surfaces (FSS) are periodic structures that have already been used for various applications such as microwave and optical frequency filters, radar absorbing materials (RAMs) and reflectors [15]. Electronic Band Gap (EBG) and Artificial Magnetic Conductors (AMCs) inspired by FSS have been used to reduce the height of antennas and the influence of the body in wearable applications [8][16]. Active switchable FSS have been proposed in the literature for system reconfiguration [17][18][19]. Several approaches have been used to change the transmission frequencies, including PIN diodes [17], varactors [20], ferrite substrates [21], MEMS [22] and optical illumination [23].

The authors have recently demonstrated the viability of using modulated FSS for RFID applications using readers based on ultra-wide band (UWB) [24][25] and FMCW [26] radars at X band. The distance between the transponder (tag) and the time-domain UWB or FMCW readers can be obtained. These transponders are therefore candidates for use in localization applications. However, in [24]- [26] the effect of the materials where the transponder is attached has not been considered, assuming that it was in free space. On the contrary, here the work is addressed at studying the effect of high-loss materials, such as the body. The originality of this paper lies in its study of modulated FSS to be placed on the body for identification and sensing. If the application does not require localization of the tag (e.g. in sensor applications) then simpler readers than the ones proposed in previous works (based on UWB or FMCW) can be used, since information about distance is not required. The reduction of the radar cross-section due to the proximity of high-loss materials and the detuning of antennas are two key problems that limit the use of wireless identification and sensing devices on the body. This problem is mitigated with the use of modulated FSS as shown in this paper, especially when increasing the number of elements. Increasing the number of dipoles in the FSS increases the radar cross section and also its bandwidth. In this work, transponders based on FSS on flexible substrate are designed and measured on the body, demonstrating their capability of sending information for identification and from sensors by backscattering communication. A typical solution in wearable antennas ([7]- [10]) is to use patch antennas or spacers to separate the antenna from the body. Using the proposed FSS, increasing the thickness of the tag and

Manuscript received May 27, 2015. This work was supported by the Spanish Government Project TEC2015-67883-R, H2020 Grant Agreement 645771–EMERGENT and the Grant BES-2012-0539802.

The authors are with the Department of Electronic, Electric and Automatic Control Engineering, Universitat Rovira i Virgili, 43007 Tarragona, Spain.

(e-mail: antonioramon.lazaro@urv.cat).

multilayer designs are not required, facilitating integration in wearable applications. The designed FSS can be scaled to other frequencies adjusting the length of the dipoles. In this work, the tags are designed in the 2.45 GHz ISM band. In this band, there is a compromise between loss and size in comparison with the UHF band (larger tag size) and the 5.8 GHz ISM band (higher body loss). In contrast with previous studies at higher frequencies (UWB or X band) where the FSS were modulated using PIN diodes, low-cost silicon varactors are used here. As consequence, the power consumption, which is an important issue in WBANs, is notably lower compared with PIN diode-based FSS designs.

This paper is structured as follows: the operating principle of the system is presented in section II, where the backscattering theory presented in [26] is used to understand the modulation the FSS on the body. Section III presents the design of the prototypes. The modulated FSS is designed and evaluated by means of full-wave simulations. Section III also describes a prototype of the temperature sensor and the reader, as a proof of concept. The FSS and the prototypes are characterized in section IV. Finally, section V contains our conclusions.

II. WIRELESS SYSTEM BASED ON FSS MODULATION

A. System description

Fig.1 shows a block diagram of the proposed system for wearable applications. It consists of a reader and semi-passive tags based on modulated FSS. In this study, the unlicensed ISM 2.45 GHz is chosen but the concept can be extended to other bands scaling the system. Compared with the UHF RFID band, the 2.45 GHz ISM band enables a reduction in the size of both the reader and tag antennas, which is an important issue in wearable applications. However, the power allowed is lower and the body losses are higher than those experienced when working with the UHF band. The transmitter is composed by a generator, with a signal that is amplified to obtain the desired power. A continuous wave (CW) illuminates the tag, which answers by modulating the backscatter of the FSS's radar cross section. The backscattered signal is demodulated using a homodyne receiver, converted to baseband with a mixer and digitized with an analog to digital converter. A bistatic topology (two antennas, one for transmission and other for reception) is used. A temperature sensor is integrated in the transponder, as a proof of concept, which modifies the frequency of a low-frequency oscillator modulating the radar cross section (RCS) of the FSS.

The free space propagation model is used to estimate the read range of the system. The received power (P_R) can be calculated as in the conventional RFID systems using the radar equation:

$$P_R = \frac{P_T G_T}{4\pi r^2} RCS_{dif} \frac{1}{4\pi r^2} \frac{\lambda^2}{4\pi} G_R \qquad (1)$$

Where r is the read range, P_T is the transmitted power, G_T and G_R are the transmission and reception antenna's gain, respectively, λ is the wavelength and RCS_{dif} is the tag differential radar cross section, given by [27]:

$$RCS_{dif} = \frac{\lambda^2}{4\pi} G^2 \left|\Delta\Gamma\right|^2 m \qquad (2)$$

In (2), G is the gain of the tag antenna, m is the modulation factor and $\Delta\Gamma$ is the difference between the reflection coefficients depending on the two impedance states used to modulate the radar cross section of the tag.

According to (1), the aim is to increase the received power and therefore the read range by maximizing the differential RCS, since the transmitted power is limited by the regulations, and the use of high-gain receiver antennas is unpractical (too directive) and expensive for WBAN applications. The conventional antennas used in passive UHF RFID tags (e.g. dipole antennas) are not appropriated when the tag is in contact with the body because its gain decreases. Furthermore, the tag is detuned due to the high permittivity of the body. Consequently, a significant drop in the power received at the tag chip is experienced. If this power is under the chip's threshold power, the tag is unable to answer the reader. In semi-passive (battery assisted, BAP) tags, this problem is mitigated because they have lower threshold powers than passive tags. However, in both cases, the reflected power experiences a significant drop when the tags are in contact with the body. One solution consists in using patch antennas, but they are not low-profile antennas, the printed area is large (increasing the cost due to the conductive inks) and they need two printing layers. The use of spacers can also be considered, but this solution is impractical in wearable applications. As an alternative, this work proposes a semi-passive tag based on a modulated FSS (semi-passive is used here to mean that the tag does not transmit RF power – it is a backscatterer).

An antenna based on an array of dipoles increases the gain with respect to a single dipole according to the array factor, consequently increasing its differential RCS, and mitigating in this the effect of the body. The FSS can achieve a large modulating bandwidth [26], and the FSS is therefore suitable for placing on parts of the body with different dielectric permittivity and also when the tag is attached to different people. The tag can be located in any position on the body, depending on the application or sensor to be integrated. In addition, FSS are one-layer printed circuits, an added value to be integrated in wearable applications.

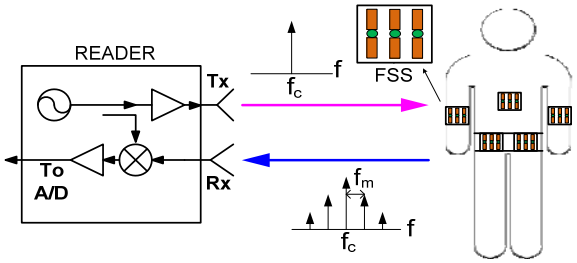

Fig. 1. Block diagram of the system, including the reader and possible locations of FSS.

B. On-body modulated frequency selective surface

The FSS unit cell is formed by dipoles loaded with diodes. PIN diodes as switching elements are sometimes used in reconfigurable FSS whereas varactor diodes are used in applications where continuous frequency tuning is required. The main problem with PIN diodes is that they need currents in the order of several mA to reduce the resistance when the diodes are in ON state. This power consumption is prohibitive in battery-assisted tags because it would dramatically reduce battery lifetime. Low cost silicon varactor diodes instead of PIN diodes are therefore chosen in order to reduce the power consumption. At 2.45 GHz, silicon devices present small parasitic components; there is therefore no need to use expensive GaAs devices. Wearable applications require flexible substrates. A liquid crystalline polymer (LCP) substrate from Rogers (Ultralam 3850) with a thickness of 100 µm is used in the prototypes. The tag modulates the incident field by switching the varactor diodes that load the FSS. The varactor diodes are reverse biased to avoid current consumption. The diodes are switched between 0V and Vcc (usually around 3 V for coin-cell battery powered devices). When the diodes are biased at 0V (ON state) they present a high capacitance, with the equivalent circuit at microwave regions a short circuit (low impedance state). Whereas the diodes are biased at Vcc (OFF state), the capacitance is considerably lower than in the first case, presenting high impedance at microwave regions. The diodes are therefore ideally equivalent to an open circuit. The load impedance of the FSS elements is thus switched between a low (ON state) or a high (OFF state) value. In order to understand the RCS modulation of the FSS on the body, the equivalent circuit in Figure 2 has been proposed. The bandpass behavior of the FSS on the body can therefore be modeled as an LC series equivalent circuit (Fig. 2b). The metallic strips are inductive, which together with the gap capacitances create a series combination of inductors with capacitors. By mounting lumped reactive elements such as varactor diodes, it is possible to tune the resonance frequency of the array. The equivalent circuit model can be extended to the case where the FSS is placed on the body (Fig.2.c). The substrate is modeled as a transmission line of length h and the body is modeled as an infinite lossy transmission line. It should be pointed out that this is only an approximate method since, if the elements of the array are long, the wave variations along the elements must be taken into account. In addition, it is only valid around the first resonance. In order to consider harmonics, additional LC resonators tuned at each resonance must be added. Nevertheless, this approach provides a good understanding of the behavior of active arrays. The impedance of an FSS made of a Perfect Electric Conductor (PEC) in free space can be represented by a series circuit consisting of an inductance L and a capacitance C_0 [28]. The resonant frequency of an FSS in the presence of a thick dielectric substrate is reduced by a factor equal to $\varepsilon_r^{1/2}$ when the dielectric is present on both sides of the FSS, and by a factor of $((\varepsilon_r+1)/2)^{1/2}$ when the dielectric is present only on one side of the FSS [29]. When an FSS is printed on a dielectric substrate, the value of the unloaded capacitor C_0 must be multiplied by the effective dielectric permittivity due to the surrounding dielectrics. If the condition of a sufficiently thick substrate is verified, the effective permittivity simply corresponds to the average of the relative permittivity of the substrate and the relative permittivity of free space [15]:

$$C = C_0 \varepsilon_{ef} \approx C_0 \frac{\varepsilon_r + 1}{2} \quad (3)$$

The loss of the body can be modeled as a series resistance [30] which reduces the quality factor of the circuit. This resistance is composed of two contributions: the resistance that models the ohmic loss and another which models the dielectric losses. Here, the ohmic loss can be neglected because its value is considerably lower than the resistor associated to dielectric loss.

The effect of the diode can be taken into account with its impedance in parallel with the capacitor. As an initial approximation, neglecting the parasitic elements of the diode, this impedance can be modeled as a variable capacitor that depends on the diode voltage. The resonant frequency of the FSS can therefore be estimated as:

$$f_0 \approx \frac{1}{2\pi\sqrt{L(C_v + C_0(\varepsilon_r + 1)/2)}} \quad (4)$$

According to (4), the resonant frequency for a FSS placed on the body is lower than in free space (ε_r=1). In addition, the tuneability is considerably lower than in free space when the FSS is on the body.

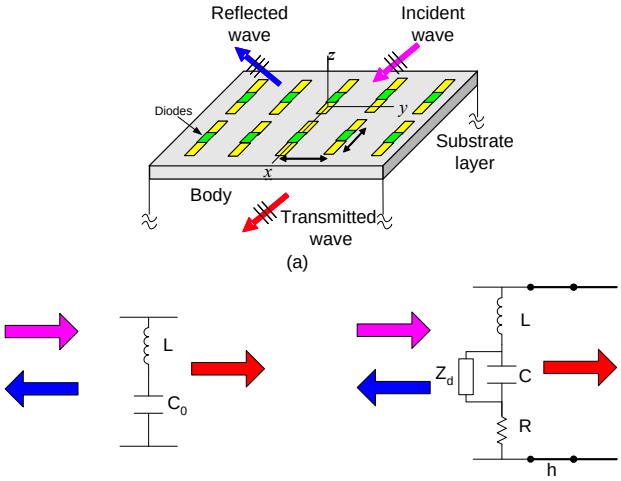

Fig. 2. (a) FSS on the body composed of dipoles loaded with diodes, (b) Equivalent circuit model of an unloaded FSS in free space, (c) Equivalent circuit model for an on-body FSS.

However, there are important differences between an active FSS in free space (or over a thin supporting substrate) and the FSS on the body. FSS in free space is known [15] to present high reflectivity when the frequency of the incident wave is close to the dipoles' resonant frequency (when the dipoles become approximately half a wavelength). Consequently, an FSS in free space loaded with ideal switching diodes presents high reflectivity (and RCS) around the dipoles' resonant frequency for the ON state (diodes are short circuits). In the other case, when the diodes are in the OFF state, the FSS in free space is like an array of dipoles whose electrical length is half of the forward-biased case. As a result, the resonant

frequency of the FSS in free space when loaded with an open circuit is about the double than that of the first case (diodes in the ON state). The FSS acts as a metallic surface (the diodes will be ON) when the length of the dipoles is designed to resonate in the centre frequency band of the application, and it will reflect the incident waves (with an electric field parallel to the dipole axis). When the diodes of the FSS are OFF, the FSS will be transparent to the incident wave. However, the diodes have parasitic elements and their behavior is different from the ideal short circuit (in the ON state) and open circuit (in the OFF state). It can be deduced from (4) that the tuning range is notably reduced.

When the FSS is attached to the body there is an important reflection of the waves on it due to high permittivity, in contrast to the case of the FSS in free space presented in the literature (see e.g. [17]-[23]) or previous works by the authors [24]-[26]. The reflectivity of the FSS is also high for frequencies outside the resonance, because a fraction of the energy is reflected and another fraction is absorbed by the human body. Nevertheless, there is a change in the reflectivity as a function of the frequency and the RCS is consequently modulated at the switching rate of the diodes. The other important effect is the reduction of the resonant frequency due to the high effective permittivity of the body, allowing a miniaturization of the FSS compared to the free-space case. In practice, the parasitic effects of the diodes have an important repercussion in the FSS's frequency response [24][26]. The modulation of the FSS is described in a previous work [26]. It is summarized here for completeness. The backscattered field has been modeled as the backscattered field of an array of antennas, composed of a sum of two terms: a structural mode (also called residual mode) and an antenna mode, or a load-independent term and a load-dependent term, respectively [31][32]:

$$\overline{E}_S = \overline{E}_{est} + \overline{E}_m \Gamma \tag{5}$$

where Γ is the complex power reflection coefficient of the diodes given by:

$$\Gamma = \frac{Z_d - Z_a^*}{Z_d + Z_a} \tag{6}$$

In (2), Z_a is the scan impedance of the FSS [15]. From (5) it is clear that the structural mode (E_{est}) cannot be used to send information, whereas the antenna mode ($E_m\Gamma$) changes with the diode impedance, Z_d. In addition, the structural mode depends on the objects where the tag is placed. The structural mode is higher than the antenna mode because the reflection on the body is larger than the tag's backscattered field by the FSS which has a smaller surface than the body. In addition, the signal coupled between the transmitter and the receiver due to the finite isolation between the antennas is often larger than the backscattered field. However, the structural mode and coupling components are converted to DC component at the output of the mixer (see fig.1). These components can therefore be separated from the information by modulating the diodes. To this end, a low-frequency square wave oscillator with oscillating frequency f_m is connected to the diodes. The complex reflection coefficient is modulated by switching the diodes that load the dipoles of the FSS. Then Γ changes between Γ_{ON} and Γ_{OFF} when the diodes are in the ON state (V=0) and OFF state (V=-Vcc), respectively. As a first approximation, the reflection coefficient is approximated by a square waveform with amplitude ΔΓ and frequency f_m. It is developed in a Fourier series:

$$\Gamma(f) = \sum_{n=-\infty}^{+\infty} c_n \delta(f - (f_c + nf_m)) \tag{7}$$

where c_n are the Fourier coefficients, and f_c is the input frequency of the incident signal that illuminates the tag. For a square waveform with duty cycle δ, the backscattered field can be written as [26]:

$$\begin{aligned} \overline{E}_S &= \left(\overline{E}_{est} + \overline{E}_m \Gamma_{avg}\right)\delta(f - f_c) \\ &+ \overline{E}_m \sum_{n\neq 0} \Delta\Gamma\gamma \left(\frac{\sin n\pi\delta}{n\pi\delta}\right) * \delta\left[f - \left(f_c + nf_m\right)\right] \end{aligned} \tag{8}$$

where $\Gamma_{avg} = (\Gamma_{ON}+\Gamma_{OFF})/2$ and $\Delta\Gamma = \Gamma_{ON}-\Gamma_{OFF}$ are the average and difference in the power reflection coefficient between ON and OFF states, respectively, δ the duty cycle of the square pulse and * the convolution product.

The first term in (8) is a non-modulated term, and it depends on the structural mode of the tag plus a constant term. The second term represents the modulated side-bands that are a function of the antenna mode, with the terms $n=\pm 1$ the main contribution (coefficients of higher amplitude in the Fourier expansion) that result in the components at the frequencies $f_c \pm f_m$. These components can therefore be used to send information from the tag to reader. The information (either ID or data from sensors) can be sent digitally, e.g. using an amplitude shift key (ASK) modulation. In this work, the information is coded in the frequency f_m which is a function of the magnitude to sense (temperature in this case). The measurement of the modulating frequency can also be used as ID for identification applications. The signal received (at $f_c \pm f_m$) in the reader can therefore be expressed as a function of the differential RCS [27]. The differential RCS [27] is the RCS due to the antenna mode, which depends on the load reflection coefficient difference ΔΓ between the two modulated states (diodes ON and OFF). The differential RCS can be expressed as:

$$\begin{aligned} RCS_{dif} &= \lim_{r\to\infty} 4\pi r^2 \frac{\left|\overline{E}_{S,ON} - \overline{E}_{S,OFF}\right|^2}{\left|\overline{E}_{in}\right|^2} = \\ \lim_{r\to\infty} 4\pi r^2 \frac{\left|\overline{E}_m c_1\right|^2}{\left|\overline{E}_{in}\right|^2} &= \left(\lim_{r\to\infty} 4\pi r^2 \frac{\left|\overline{E}_m\right|^2}{\left|\overline{E}_{in}\right|^2}\right)\left|\Delta\Gamma\right|^2 m \end{aligned} \tag{9}$$

where m is a modulating factor that can be obtained from (8) as $m=|c_1|^2/|\Delta\Gamma|^2$. Equation (9) is similar to the well-known differential RCS used in RFID tags [27].

III. PROTOTYPE DESIGN

A. FSS design

From the theory presented in the last section, the most important property of the FSS to be used in semi-passive tags is the differential RCS. To this end, some simulations using Ansoft HFSS have been conducted. The FSS can be located in different parts of the body, such as the arms, shoulders, chest, etc. It is assumed here that the FSS is attached to the arm. It is expected that FSS presents high reflectivity for the ON state (low impedance state) where the dipole length will be close to half-wavelength at the center frequency (f_c=2.45 GHz):

$$L \approx \frac{1}{2}\frac{c}{\sqrt{\varepsilon_{ref}}\, f_c} \tag{10}$$

Where the effective permittivity (ε_{ref}) will be the average between the air and the effective permittivity of the body, $\varepsilon_{ref,body}$:

$$\varepsilon_{ref} \approx \frac{1+\varepsilon_{ref,body}}{2} \tag{11}$$

In order to avoid grating lobes, the period (separation between the dipoles) must be smaller than half of the wavelength [15]. The dielectric properties of the body tissues have been studied based on the measurements provided in [33]. It is assumed that the arm can be approximated as a multilayer structure of 1.5-mm thick skin, a fat tissue of 1.5 mm and a layer of muscle of 15 mm. The relative permittivity and dissipation loss tangent values for each tissue at 2.45 GHz taken from [28] are listed in table I. In order to estimate the effect of the body and to adjust the dimensions of the FSS the effect of the arm curvature is neglected as the first approximation.

Low-cost silicon varactors from Skyworks SMV1247-079LF are used and inserted as lumped RLC boundary conditions in the HFSS simulations. Their capacitance is 6.5 pF and 0.95 pF for V=0 (ON state) and V=-3V (OFF state), respectively. The parasitic inductance and resistance are 0.7nH and 2 Ω, respectively. The FSS will be implemented using a 100 µm thickness Ultralam 3850 substrate. 10 kΩ 0605 SMD resistors are connected at the end of the arms of the dipole to feed the diodes and block the RF signal. The feed line is orthogonal to the dipole direction to avoid interference in the backscattered field. The dipole length is adjusted to resonate at about 2.45 GHz. Its length and width are 25.6 mm and 1 mm respectively. Fig.3(a) shows a schema of the FSS with 5 dipoles and Fig.3(b) the FSS on the arm.

TABLE I
DIELECTRIC PROPERTIES OF ARM USED IN SIMULATIONS

Layer	Thickness (mm)	Relative Permittivity	Dissipation Loss tangent
Skin	1.5	42.8	0.27
Fat	1.5	5.3	0.14
Muscle	15	52.6	0.24

The effective permittivity of the body must be known in order to adjust the resonant frequency of the FSS using (11). However, it is difficult to analytically determine the value for multilayer structures as the considered here. The resonant frequency is therefore adjusted with electromagnetic simulations. First a single dipole is considered. Fig. 4 shows the simulated RCS of the structure, considering a single dipole including the diode (two states) over the arm. The strong structural mode makes it difficult to see the field backscattered at the dipole. In order to remove the effect of the background, a simulated scattered field without the dipole (background) is performed and it is then subtracted from the simulations for the two states (see graphs with makers in Fig.4). As in the case of FSS in free space [25][26], the differences between the two states depending on the differences in the reflection coefficients and the diode parasitic elements play an important role. The differential RCS for different number of dipoles has been simulated in order to investigate the effect of the number of dipoles. The dipoles' length is fixed to L=25.6 mm and the spacing between them is 10.24 mm.

The next step is to simulate a periodic infinite structure. To that end, periodic boundary conditions are considered and the Floquet port is defined in Ansoft HFF (see fig. 5). The simulated results can be shown in Fig.6. The reflection coefficient (S_{11}) is shown for the two diodes states in Fig. 6a. The differential RCS (9) is then estimated as:

$$RCS_{dif}(dB) = \frac{4\pi}{\lambda^2} A^2 \left| S_{11,ON} - S_{11,OFF} \right|^2 m \tag{12}$$

where the term $4\pi/\lambda^2 A^2$ is the RCS of a plate of area A, $S_{11,ON}$ and $S_{11,OFF}$ is the reflection coefficient for ON and OFF state, respectively, and m is the modulation coefficient. Fig. 6b shows the differential RCS considering the area covered by seven dipoles. As the modulation coefficient depends on the waveform, m=1 is considered in this figure to independize from the modulating waveform. Compared with the simulation of only one dipole, except for a small shift in the resonant frequency, it can be observed that the maximum differential RCS is around 2.4 GHz, and the -10 dB bandwidth is from 2.1 GHz to 2.7 GHz covering the 2.45 GHz ISM band.

In wearable applications, the area of the FSS is limited by the maximum size allowed. Although this area can be relatively large if the FSS is integrated in the textile, in other cases, e.g. if the FSS is attached on the arm, then the maximum size is limited to a small number of cells or dipoles. In these cases, the structure seems to be an array of dipoles. In order to investigate the differences when the structure is truncated with the case of an infinite periodic structure, some simulations changing the number of dipoles were conducted. Fig. 7 shows the differential RCS obtained from the difference of the backscattered fields between the ON and OFF states, according to the number of dipoles. This difference is the differential RCS (9) when a modulating factor of 1 is assumed. It can be observed that the differential RCS and its bandwidth increase with the number of dipoles, although the maximum of the differential RCS is frequency shifted to lower frequencies. This shift can be easily corrected in practice by scaling the length of the dipoles.

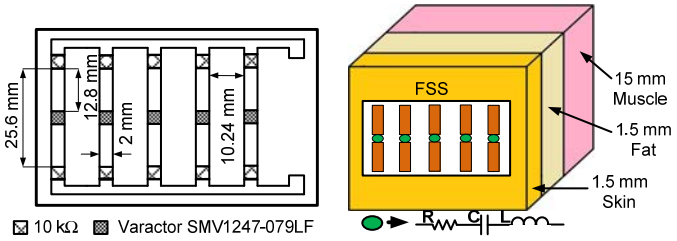

Fig.3. (a) Schema of a FSS with 5 dipoles and (b) stack of layers in HFSS software for the simulation of the FSS on the arm.

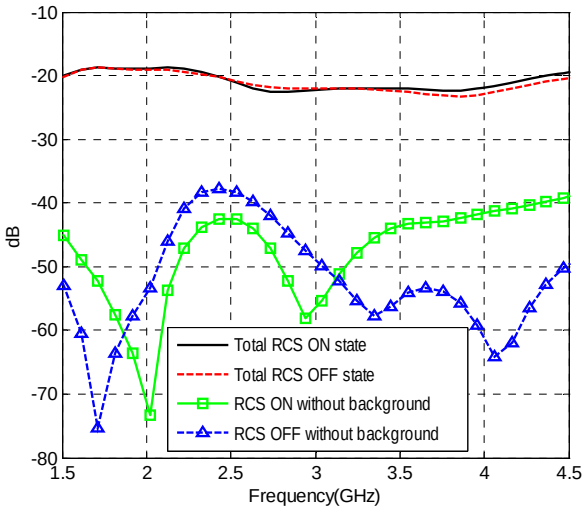

Fig. 4. Simulation of total RCS of a dipole for the two diode states (-ON, --OFF) with and without the background (Δ ON, □ OFF) for a single dipole (length L=25.6 mm).

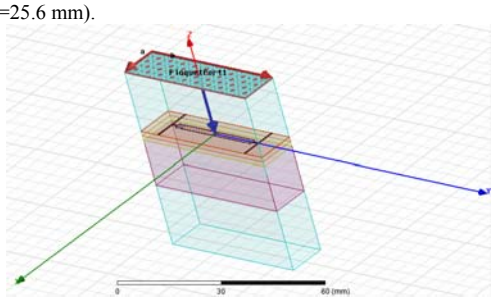

Fig.5. Schema implemented in Ansoft HFSS to simulate the FSS using Floquet ports.

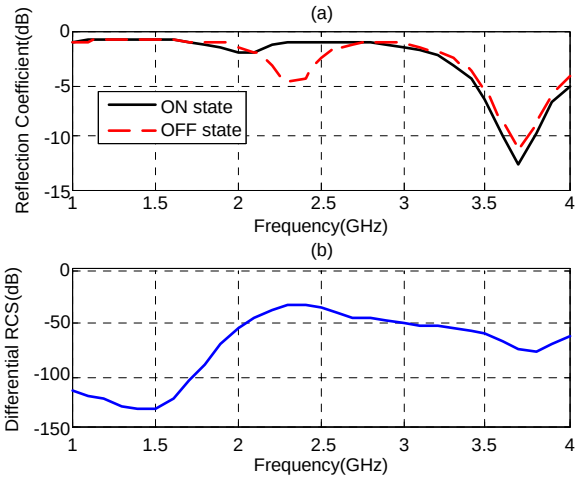

Fig.6. (a) Simulated reflection coefficient for the two diode states. (b) Simulated differential RCS of a structure composed of seven unit cells.

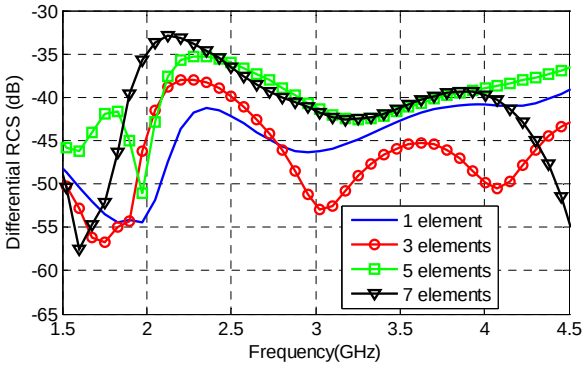

Fig. 7. Simulation of the differential RCS between the two diode states as a function of the frequency for a different number of elements (length L=25.6 mm, spacing 10.24 mm).

B. Temperature sensor design

As a proof of concept, an FSS composed of 7 dipoles is used as a transponder of a temperature sensor. The FSS is connected to a low-frequency oscillator based on the 555 timer configured as astable (Fig.8). A low power version (Intersil ICM7555 [34]) that only draws 60 µA from a 3V button type battery is used. The diode anodes are connected to the battery voltage and the cathodes are connected to the oscillator output (pin 3). The diodes are therefore switched between -3V when the oscillator output is 3V and 0V when the output of the oscillator is in low state. The oscillation frequency f_m depends on the RC time constant as [34]:

$$f_m = \frac{1}{1.4RC} \tag{13}$$

where R is the oscillator resistance between pin 3 and 2 and C is the capacitance between pin 6 and ground. In this case, the R is a variable resistance that depends on the temperature: a negative temperature coefficient (NTC) thermistor (AVX NB20J00472) connected according to the schema in Fig. 8. The oscillation frequency can be adjusted to the desired frequency range within the frequency range allowed by the AD converter given by the Nyquist criterion to avoid aliasing (less than half of the sampling frequency). Multiple sensors can be measured choosing different frequency ranges. The capacitor value used here is 39 nF, which translates into a modulating frequency range between 5 kHz and 7 kHz around the body temperature. The Steinhart–Hart equation [35] is widely used to model the resistance. The thermistor manufacturer uses the first-order approximation:

$$\frac{1}{T} \approx \frac{1}{T_0} + \frac{1}{\beta} \ln \frac{R}{R_0} \tag{14}$$

where T is the temperature in K, R_0=4.7 kΩ is the nominal resistance at T_0=298 K, and β=3480 K is the Steinhart–Hart parameter given in the thermistor datasheet.

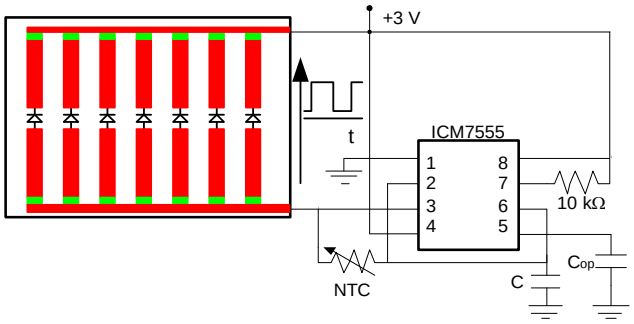

Fig.8. Schema of the oscillator with NTC resistor.

C. *Reader prototype*

A custom software defined radio (SDR) reader prototype based on the schema of Fig.1 has been designed. The signal from a PLL frequency synthesizer (Minicircuits KSN-2450A-119+) is amplified with a Minicircuits GAL84+ and it is connected to the transmitter's antenna. A microcontroller is used to program the frequency synthesizer. The output power is 18 dBm. A microcontroller (Arduino UNO board) is used to program the synthesizer and to bias the RF front-end. One part of the power is coupled to the local oscillator of the mixer (Minicircuits LRMS-30J), which down converts the signal arriving in the receiver. The intermediate frequency (IF) power at the mixer's output is amplified using two operational amplifiers with an overall gain of 50 dB and a filter with cut-off frequency of 20 kHz connected in cascade. The output is sampled using the analog-to-digital converter (ADC) of a sound card. Fig. 9 is a photograph of the prototype.

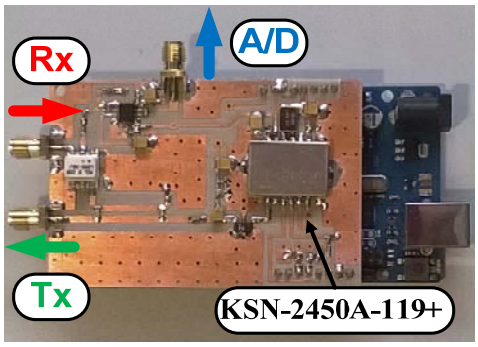

Fig.9. Photograph of the reader.

IV. EXPERIMENTAL RESULTS

A. *FSS characterization*

This section shows the experimental results. The measurements are performed in the laboratory (indoor environment). A photograph of the system used for the characterization of the FSS is shown in Fig. 10. The FSS is modulated with a low-frequency generator (Agilent 33521A) that generates a 7 kHz, 2.5Vpp signal. A signal generator (Rodhe & Schwarz SMAF100) is connected to a wideband antenna (Geozondas AU-1.0G4.5GR from 1.5 to 4.5 GHz) and it is used to illuminate the FSS transmitting 10 dBm. The reflected signal is received through another identical antenna and it is measured with a spectrum analyzer (Rodhe&Schwarz FSP30). Some prototypes of FSS with different number of elements have been manufactured. For example, Fig.11 shows the prototype of a FSS with 7 elements. The dipole length is 25.6 mm and the spacing between dipoles 10.24 mm. Two cases are compared in order to evaluate the detuning effect due to the arm. In the first case, a bracer is used as a spacer of 5 mm between the FSS and the arm, and in the other case the tag is placed directly around the arm. Fig. 12 shows an example of the received spectrum at 2.45 GHz as a function of the offset frequency from the carrier for various distances. A strong central peak due to the coupling signal between the transmitter and receiver can be observed. Two sideband peaks at the modulating frequency (7 KHz in this case), whose amplitude decreases with the distance, are observed.

The measured received power as a function of the frequency for different number of dipoles is shown in Fig. 13. The differences due to the antenna gain are corrected in order to better appreciate the effect of the frequency behavior of the FSS. Microwave absorbers are used to avoid deep frequency fadings generated by multipath interference that could mask the measurements. A flat response from 2 GHz to 3.5 GHz is observed for FSS directly in contact with the body, whereas when the spacer is used the response is shifted to 4 GHz and the bandwidth is smaller than in the former case. Due to the body losses, the received level when the FSS is in contact with the arm is between 5 and 10 dB lower than when the spacer is used. The received level increases with the number of dipoles, as the simulations predicted. The dielectric properties of the arm can change between individuals or depend on the body part chosen. The system offers a high level of robustness in detuning problems, thanks to the large bandwidth achieved. When FSS are attached to thick textile materials, their average thickness directly intervenes in the FSS working frequency, but it can be easily modified by adjusting the length of the dipoles. A phantom has also been used to emulate the arm, based on a cylindrical piece of ham (8 cm of diameter) (Fig.10). Fig.14 shows measurements of the power received from an FSS with 7 elements placed on the arm and on the phantom. Good agreement is obtained between the two situations. In order to study the angular behavior, the FSS placed on the phantom is mounted on a rotary table connected to a stepper motor. Fig. 15 shows the received power as a function of the angle.

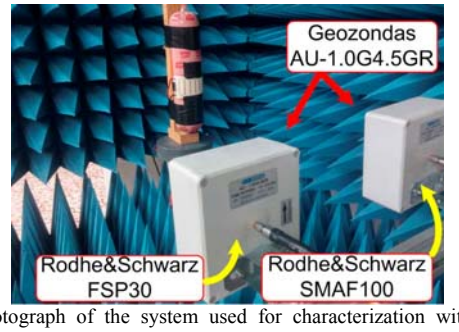

Fig.10. Photograph of the system used for characterization with the FSS placed on a phantom.

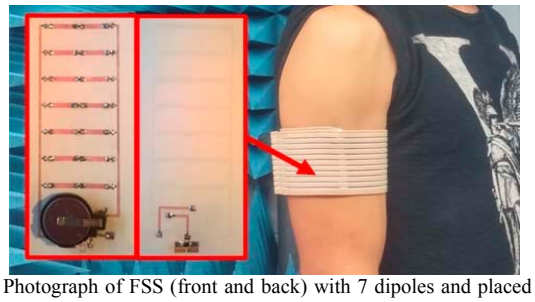

Fig.11. Photograph of FSS (front and back) with 7 dipoles and placed on the arm.

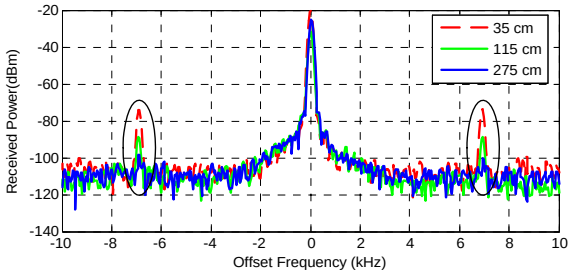

Fig.12. Received power measured with the spectrum analyzer as a function of the offset frequency from the transmitted carrier for different distances.

In order to estimate the read range in real environments, measurements of the backscattered power in an indoor environment (laboratory) were taken as a function of the distance for a tag composed of 7 dipoles. Fig. 16 shows the measured received power as a function of the distance in order to estimate the read range. The transmitter power is adjusted to comply with the European regulation ERC-REC 70-03 (EIRP 20 dBm). The measurements are compared with simulations using the free-space model given in (1) at 2.45 GHz, and considering the RCS difference between the ON and OFF states of -40 dB, according to the simulated results in Fig. 5 and a modulating factor of $1/\pi^2$, which corresponds to a modulating square waveform with a duty-cycle of 50% (8-9). Additionally, USA regulation (FCC Part 15, maximum EIRP 30 dBm) is also considered and compared here. Good agreement is observed for distances below 1 m, validating the simulated differential RCS. The effect of multipath is observed for higher distances. In this case there is a ripple with the distance which depends on the frequency. This effect was observed in UHF RFID applications [36] and other indoor environments. For very small distances, the tag is in Light-of-Sight (LOS) conditions, but when the distance between the reader and the tag increases, the reader antenna illuminates other objects near the tag. The multipath contributions due to reflections in the objects then tend to create an increase in received power because the difference in the path length difference is small. However, the channel is frequency selective because the multipath contribution sometimes produces destructive interferences. The result is the ripple in the received power. The channel must therefore be statistically modeled for distances greater than 1 m. The free space model can be used to predict the average power level. For distances higher than 3 m, the received power is under the sensitivity of the spectrum analyzer (around -100 dBm for the setup used). In recent works in the literature based on passive epidermal UHF RFID [37][38], the read range achieved with tags attached to the body is 0.8 m [37] and 0.5 m when temperature-sensing microchips were included, and 2 m without sensing chip [38], respectively. The read range in this work is considerably higher and uses less transmitter lower power. The main reason is the limitation on the uplink link budget between the reader and tag [36], since the passive RFID tags require a minimum received power to wake up the internal circuitry because the tag is fed from the rectified voltage from the incoming wave. This threshold power is typically between -15 dBm and -21 dBm (Monza R6, from Impinj, USA), depending on the commercial chip used. These sensitivities are lower when sensing capabilities are included in the chip (e.g. -9 dBm for EM4325 from EM Microelectronics, Switzerland). In semi-passive RFID systems such as the one presented here, the read range limitation is the sensitivity of the reader. Since low transmitted power is used, the typical coupling between antennas (better than 25 dB) or the isolation of a typical circulator (in the case of a monostatic reader) is enough to protect from the transmitter leakage by adding attenuators at the input of the mixer. The sensitivity of the reader can therefore be considerably higher (better than -100 dBm) than the typical -60 dBm to -80 dBm achieved in commercial UHF readers. In addition, the effect of losses due to the body is partially compensated by the antenna gain array factor, and the backscattered power is therefore higher compared to RFID systems based on one dipole-like antenna, allowing for this higher read range.

The problem of multipath interference can be mitigated using spatial diversity techniques or frequency hopping techniques. The first solution is often implemented in UHF readers in dock doors, where two or more channels (antennas) can be used to reduce the effect of fading due to multipath interference. In addition, the increased bandwidth allows the frequency carrier finding the channel to be changed, with higher received power such as in Bluetooth devices.

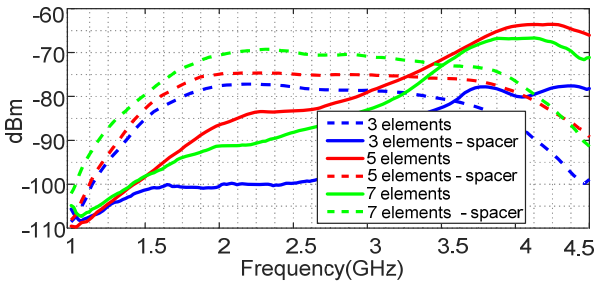

Fig.13. Measured received power for FSS with different number of dipoles in contact with the arm (dashed lines) and with the spacer (solid lines).

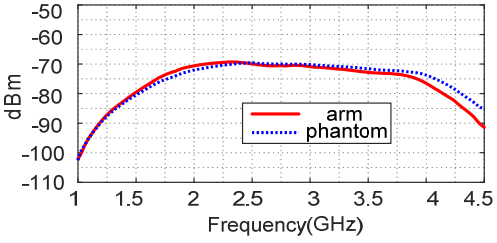

Fig. 14. Measured received power for FSS with 7 dipoles in contact with the arm (solid line) and with the phantom (dotted line).

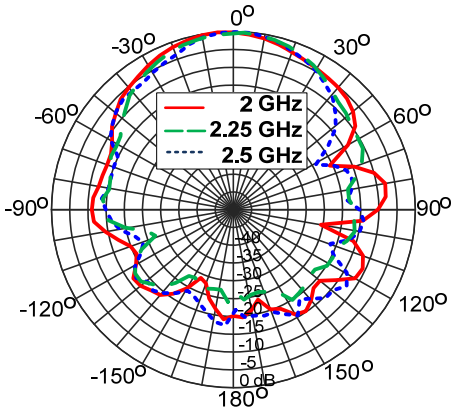

Fig.15. Normalized measured power as a function of angle at 2, 2.25 and 2.5 GHz.

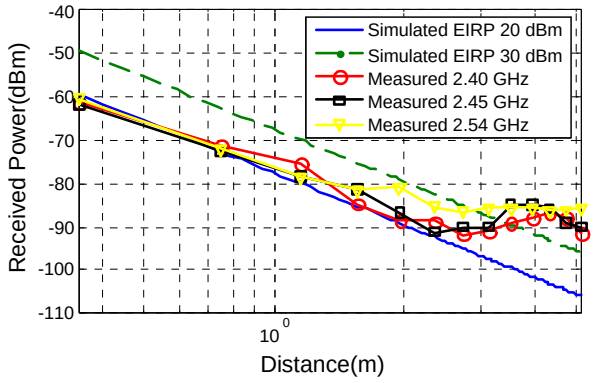

Fig.16. Measured and simulated received power for tag composed by 7 dipoles on the arm.

B. Measurement of the temperature sensor

Fig. 17 shows the baseband spectrum obtained from the Fourier transform of the measured signal using the reader at 3 m distance with the tag composed by 7 dipoles in contact with the arm. The chirp Z-transform algorithm with a Hamming window is used to achieve the appropriated frequency resolution. A signal-to-noise ratio of about 10 dB is obtained, and that is enough to detect the signal. The temperature is obtained by measuring the frequency of the peak. The sensor is heated with a heat gun and measured while cooling. The NTC resistance (obtained with a multimeter) and the frequency of the peak are measured simultaneously. The temperature of the NTC is obtained from the measured resistance using the calibration curve given by the NTC manufacturer. Fig. 18 shows the relationship between the measured temperature from the calibration curve and the measured modulation frequency for a tag made of 7 dipoles placed on the arm. The theoretical model (13-14) is also compared with good agreement. A nearly linear relationship and a correlation coefficient of 98.8% are obtained.

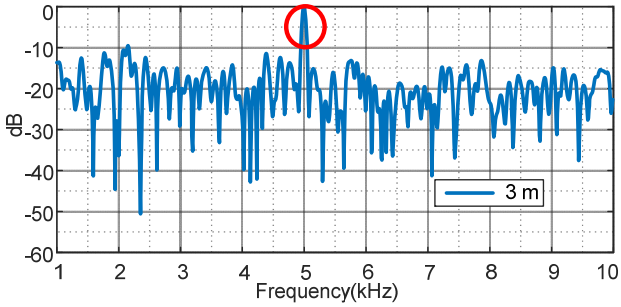

Fig.17. Baseband spectrum obtained from Fourier Transform of the sampled signal in reception for tag composed by 7 dipoles on the arm.

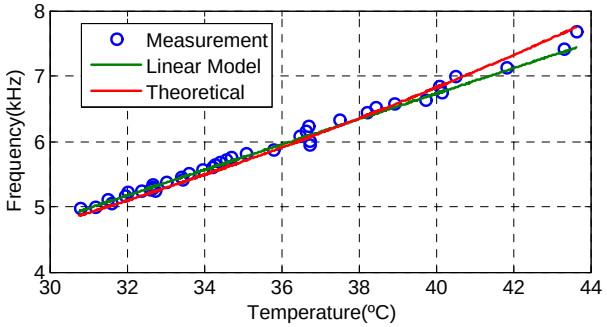

Fig.18. Detected modulation frequency as function of the NTC temperature for tag composed by 7 dipoles on the arm at a distance of 3 m.

V. Conclusions

This work has studied the feasibility of using modulated frequency surfaces (FSS) for on-body applications. The radar cross section has been modulated using low-cost reverse-biased varactors; the power consumption of the semi-passive FSS is therefore very low. The communication between the tag and the reader is performed by the backscattering technique. The effect of the losses of the body has been investigated both theoretically and experimentally. A loss of between 5 and 10 dB in the backscattered power is experimentally observed when the FSS is in contact with the body. However, greater bandwidth and a flatter response of the FSS were obtained. This increased bandwidth gives the system robustness when dealing with variations in the dielectric properties of the body, and makes it independent from the part of the body where the FSS is attached.

A prototype of an analog frequency modulated (FM) temperature sensor based on a low-frequency oscillator connected to the FSS has been presented as a proof of concept. Read ranges up to 3 m in indoor environments have been obtained. The tag presents low power consumption (60 µA at 3V), which is much lower than other wireless sensors based on transmitters (e.g. a typical Bluetooth 4.0 needs more than 7 mA at 3V during reception or transmission). These results open the door to more complex RFID tags and sensors based on FSS for on-body applications which integrate microcontrollers and more sophisticated sensors depending on the application.

REFERENCES

[1] E. Montón, J. F. Hernandez, J. M. Blasco, T. Hervé, J. Micallef, I. Grech, A. Brincat, and V. Traver, "Body area network for wireless patient monitoring," *IET Commun.*, vol. 2, no. 2, p. 215, 2008.

[2] P. D. Mitcheson, E. M. Yeatman, G. K. Rao, A. S. Holmes, and T. C. Green, "Energy harvesting from human and machine motion for wireless electronic devices," *Proc. IEEE*, vol. 96, no. 9, pp. 1457–1486, 2008.

[3] P. S. Hall and Y. Hao, "Antennas and propagation for body centric communications," in *First European Conference on Antennas and Propagation, 2006. EuCAP 2006*, 2006, pp. 1–7.

[4] G. A. Conway and W. G. Scanlon, "Antennas for Over-Body-Surface Communication at 2.45 GHz," *IEEE Trans. Antennas Propag.*, vol. 57, no. 4, pp. 844–855, Apr. 2009.

[5] S. Manzari, S. Pettinari, and G. Marrocco, "Miniaturised wearable UHF-RFID tag with tuning capability," *Electron. Lett.*, vol. 48, no. 21, p. 1325, 2012.

[6] C. Occhiuzzi, S. Cippitelli, and G. Marrocco, "Modeling, Design and Experimentation of Wearable RFID Sensor Tag," *IEEE Trans. Antennas Propag.*, vol. 58, no. 8, pp. 2490–2498, Aug. 2010.

[7] M. Klemm and G. Troester, "Textile UWB Antennas for Wireless Body Area Networks," *IEEE Trans. Antennas Propag.*, vol. 54, no. 11, pp. 3192–3197, Nov. 2006.

[8] S. Zhu and R. Langley, "Dual-Band Wearable Textile Antenna on an EBG Substrate," *IEEE Trans. Antennas Propag.*, vol. 57, no. 4, pp. 926–935, Apr. 2009.

[9] N. H. M. Rais, P. J. Soh, F. Malek, S. Ahmad, N. B. M. Hashim, and P. S. Hall, "A review of wearable antenna," in *Antennas Propagation Conference, 2009. LAPC 2009. Loughborough*, 2009, pp. 225–228.

[10] A. Baroni, H. Rogier, and P. Nepa, "Wearable active Sierpinski fractal antenna for off-body communication," in *2015 IEEE-APS Topical Conference on Antennas and Propagation in Wireless Communications (APWC)*, 2015, pp. 642–645.

[11] A. Lea, P. Hui, J. Ollikainen, and R. G. Vaughan, "Propagation Between On-Body Antennas," *IEEE Trans. Antennas Propag.*, vol. 57, no. 11, pp. 3619–3627, Nov. 2009.

[12] E. Reusens, W. Joseph, B. Latre, B. Braem, G. Vermeeren, E. Tanghe, L. Martens, I. Moerman, and C. Blondia, "Characterization of On-Body Communication Channel and Energy Efficient Topology Design for Wireless Body Area Networks," *IEEE Trans. Inf. Technol. Biomed.*, vol. 13, no. 6, pp. 933–945, Nov. 2009.

[13] Q. Wang, T. Tayamachi, I. Kimura, and J. Wang, "An On-Body Channel Model for UWB Body Area Communications for Various Postures," *IEEE Trans. Antennas Propag.*, vol. 57, no. 4, pp. 991–998, Apr. 2009.

[14] A. A. Serra, P. Nepa, G. Manara, and P. S. Hall, "Diversity Measurements for On-Body Communication Systems," *IEEE Antennas Wirel. Propag. Lett.*, vol. 6, pp. 361–363, 2007.

[15] B. A. Munk, *Frequency Selective Surfaces: Theory and Design*. John Wiley & Sons, 2005.

[16] F. Costa, S. Genovesi, and A. Monorchio, "On the Bandwidth of High-Impedance Frequency Selective Surfaces," *IEEE Antennas Wirel. Propag. Lett.*, vol. 8, pp. 1341–1344, 2009.

[17] A. Tennant and B. Chambers, "Adaptive radar absorbing structure with PIN diode controlled active frequency selective surface," *Smart Mater. Struct.*, vol. 13, no. 1, p. 122, Feb. 2004.

[18] T. K. Chang, R. J. Langley, and E. A. Parker, "Active frequency-selective surfaces," *IEE Proc. - Microw. Antennas Propag.*, vol. 143, no. 1, p. 62, 1996.

[19] B. Sanz-Izquierdo, E. A. Parker, J.-B. Robertson, and J. C. Batchelor, "Tuning technique for active FSS arrays," *Electron. Lett.*, vol. 45, no. 22, p. 1107, 2009.

[20] C. Mias, "Varactor-tunable frequency selective surface with resistive-lumped-element biasing grids," *IEEE Microw. Wirel. Compon. Lett.*, vol. 15, no. 9, pp. 570–572, Sep. 2005.

[21] E. A. Parker and S. B. Savia, "Active frequency selective surfaces with ferroelectric substrates," *Microw. Antennas Propag. IEE Proc.*, vol. 148, no. 2, pp. 103–108, Apr. 2001.

[22] B. Schoenlinner, A. Abbaspour-Tamijani, L. C. Kempel, and G. M. Rebeiz, "Switchable low-loss RF MEMS Ka-band frequency-selective surface," *IEEE Trans. Microw. Theory Tech.*, vol. 52, no. 11, pp. 2474–2481, Nov. 2004.

[23] J. C. Vardaxoglou, "Optical switching of frquency selective surface bandpass response," *Electron. Lett.*, vol. 32, no. 25, p. 2345, 1996.

[24] A. Lazaro, A. Ramos, D. Girbau, and R. Villarino, "A Novel UWB RFID Tag Using Active Frequency Selective Surface," *IEEE Trans. Antennas Propag.*, vol. 61, no. 3, pp. 1155–1165, Mar. 2013.

[25] A. Lazaro, R. Villarino, A. Ramos, and D. Girbau, "Active frequency selective surface for time-domain UWB RFID applications," in *Microwave Conference (EuMC), 2013 European*, 2013, pp. 136–139.

[26] A. Lazaro, J. Lorenzo, R. Villarino, and D. Girbau, "Backscatter Transponder Based on Frequency Selective Surface for FMCW Radar Applications," Radioengineering, vol. 23, no. 2, Jun. 2014.

[27] P. V. Nikitin, K. S. Rao, S. F. Lam, V. Pillai, R. Martinez, and H. Heinrich, "Power reflection coefficient analysis for complex impedances in RFID tag design," *IEEE Trans. Microw. Theory Tech.*, vol. 53, no. 9, pp. 2721–2725, 2005.

[28] O. Luukkonen, C. Simovski, G. Granet, G. Goussetis, D. Lioubtchenko, A. V. Raisanen, and S. A. Tretyakov, "Simple and Accurate Analytical Model of Planar Grids and High-Impedance Surfaces Comprising Metal Strips or Patches," *IEEE Trans. Antennas Propag.*, vol. 56, no. 6, pp. 1624–1632, Jun. 2008.

[29] P. Callaghan, E. Parker, and R. Langley, "Influence of supporting dielectric layers on the transmission properties of frequency selective surfaces," *Antennas Propag. IEE Proc. H - Microw.*, vol. 138, no. 5, pp. 448–454, Oct. 1991.

[30] F. Costa and A. Monorchio, "Closed-Form Analysis of Reflection Losses in Microstrip Reflectarray Antennas," *IEEE Trans. Antennas Propag.*, vol. 60, no. 10, pp. 4650–4660, Oct. 2012.

[31] R. E. Collin, "The receiving antenna," *Antenna Theory*, vol. 1, pp. 123–133, 1969.

[32] R. B. Green, "The general theory of antenna scattering ElectroScience Laboratory," *Columb. OH Rep*, pp. 1223–17, 1963.

[33] S. Gabriel, R. W. Lau, and C. Gabriel, "The dielectric properties of biological tissues: II. Measurements in the frequency range 10 Hz to 20 GHz," *Phys. Med. Biol.*, vol. 41, no. 11, p. 2251, 1996.

[34] ICM7555 Datasheet, Intersil, Aug. 24, 2006.

[35] J. S. Steinhart and S. R. Hart, "Calibration curves for thermistors," *Deep Sea Res. Oceanogr. Abstr.*, vol. 15, no. 4, pp. 497–503, Aug. 1968.

[36] A. Lazaro, D. Girbau, and D. Salinas, "Radio Link Budgets for UHF RFID on Multipath Environments," *IEEE Trans. Antennas Propag.*, vol. 57, no. 4, pp. 1241–1251, Apr. 2009.

[37] M. A. Ziai and J. C. Batchelor, "Temporary On-Skin Passive UHF RFID Transfer Tag," *IEEE Trans. Antennas Propag.*, vol. 59, no. 10, pp. 3565–3571, Oct. 2011.

[38] C. Occhiuzzi, A. Ajovalasit, M. A. Sabatino, C. Dispenza, and G. Marrocco, "RFID epidermal sensor including hydrogel membranes for wound monitoring and healing," in *2015 IEEE International Conference on RFID (RFID)*, 2015, pp. 182–188.

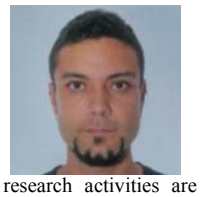

Javier LORENZO was born in Reus, Spain, in 1978. He received the Telecommunications Technical Engineering degree and MS in Electronics Engineering from Universitat Rovira i Virgili, Tarragona, Spain, in 2009 and 2011 respectively. Since September 2011 he is a PhD researcher at Universitat Rovira i Virgili, Tarragona, Spain. His research activities are oriented to microwave devices and systems, with emphasis on UWB, RFIDs, and wireless sensors.

Antonio Lázaro (M'07) was born in Lleida, Spain, in 1971. He received the M.S. and Ph.D. degrees in telecommunication engineering from the Universitat Politècnica de Catalunya (UPC), Barcelona, Spain, in 1994 and 1998, respectively. He then joined the faculty of UPC, where he currently teaches a course on microwave circuits and antennas. Since July 2004, he is a Full-Time Professor at the Department of Electronic Engineering, Universitat Rovira i Virgili (URV), Tarragona, Spain. His research interests are microwave device modeling, on-wafer noise measurements, monolithic microwave integrated circuits (MMICs), low phase noise oscillators, MEMS, RFID, UWB and microwave systems.

Ramon Villarino received the Telecommunications Technical Engineering degree from the Ramon Llull University (URL), Barcelona, Spain in 1994, the Senior Telecommunications Engineering degree from the Polytechnic University of Catalonia (UPC), Barcelona, Spain in 2000 and the PhD from the UPC in 2004. During 2005-2006, he was a Research Associate at the Technological Telecommunications Center of Catalonia (CTTC), Barcelona, Spain. He worked at the Autonomous University of Catalonia (UAB) from 2006 to 2008 as a Researcher and Assistant Professor. Since January 2009 he is a Full-Time Professor at Universitat Rovira i Virgili (URV). His research activities are oriented to radiometry, microwave devices and systems, based on UWB, RFIDs and frequency selective structures using MetaMaterials (MM).

David Girbau (M'04, SM'13) received the BS in Telecommunication Engineering, MS in Electronics Engineering and PhD in Telecommunication from Universitat Politècnica de Catalunya (UPC), Barcelona, Spain, in 1998, 2002 and 2006, respectively. From February 2001 to September 2007 he was a Research Assistant with the UPC. From September 2005 to September 2007 he was a Part-Time Assistant Professor with the Universitat Autònoma de Barcelona (UAB). Since October 2007 he is a Full-Time Professor at Universitat Rovira i Virgili (URV). His research interests include microwave devices and systems, with emphasis on UWB, RFIDs, RF-MEMS and wireless sensors.